Hybrid M-mode-like OCT imaging of three-dimensional microvasculature *in vivo* using reference-free processing of complex valued B-scans

Lev A. Matveev,[1,2,3,*] Vladimir Yu. Zaitsev,[1,2,3] Grigory V. Gelikonov,[1,2] Alexandr L. Matveyev,[1,2] Alexander A. Moiseev,[1] Sergey Yu. Ksenofontov,[1] Valentin M. Gelikonov,[1,2,3] Marina A. Sirotkina,[2] Natalia D. Gladkova,[2] Valentin Demidov,[4] and Alex Vitkin[2,4]

[1]*Institute of Applied Physics RAS, 60390, Ulyanov St., 46, Nizhny Novgorod, Russia*

[2]*Nizhny Novgorod State Medical Academy, 603005, Minin and Pozharsky Sq., 10/1, Nizhny Novgorod, Russia*

[3]*Nizhny Novgorod State University, 603950, Gagarina Ave., 23, Nizhny Novgorod, Russia*

[4]*University of Toronto and University Health Network, M5G 2M9, 610 University Ave., Toronto, Ontario, Canada*

**Corresponding author: lionnn52rus@mail.ru*

Received November 5, 2014; revised January 26, 2015; accepted February 3, 2015; posted March 3, 2015 (Doc. ID 226143); published March 27, 2015

We propose a novel OCT-based method for visualizing microvasculature in three-dimension using reference-free processing of individual complex valued B-scans with highly overlapped A-scans. In the lateral direction of such a B-scan, the amplitude and phase of speckles corresponding to vessel regions exhibit faster variability and, thus, can be detected without comparison with other B-scans recorded in the same plane. This method combines elements of several existing OCT angiographic approaches and exhibits: (1) enhanced robustness with respect to bulk tissue motion with frequencies up to tens of Hz, (2) resolution of microcirculation images equal to that of structural images, and (3) possibility of quantifying the vessels in terms of their decorrelation rates.

OCIS codes: (170.3880) Medical and biological imaging; (170.4500) Optical coherence tomography; (100.2000) Digital image processing; (030.6140) Speckle; (170.6935) Tissue characterization; (280.2490) Flow diagnostics.

http://dx.doi.org/10.1364/OL.40.001472

The need for increased information content in optical coherence tomography (OCT) of biological tissues has been exemplified by recent efforts to complement conventional structural images with additional contrast mechanisms, such as polarization-sensitive measurements and elastographic imaging [1–3]; studies of rheological/relaxational characteristics [4,5] and microvasculature characterization [6–20] as summarized in recent reviews [21,22]. Many vasculature imaging methods detect flow via phase-resolved Doppler effects, including either detailed quantification of flow profiles (e.g., [6]) or at least flow direction and approximate grading of flow velocities (power-Doppler approach [8,13]). In these methods, the Doppler frequency shift is estimated by comparing phases of adjacent A-scans. Closely related modified angiographic techniques employ additional modulation to ensure nonzero Doppler shift, even from motionless tissue, and/or advanced filtering procedures to better single out moving scatterers from nearly motionless surrounding tissue [8,9,11,16].

Another group of angiographic methods (e.g., [12,14,15]) uses temporal variability of structural B-scan speckle patterns due to the motion of scatterers in the liquid, comprising both collective flow and Brownian motion [14]. For mapping regions of increased speckle-texture variability, various analyses can be used, e.g., correlation mapping or (CM) [12] or speckle variance (SV) methods [14,15]. The common feature of these approaches is that they compare several consecutive B-scans obtained from the same location. However, the time of B-scan acquisition is typically two–three orders of magnitude longer than that of individual A-lines. For a typical interval between B-scans of ~tens of milliseconds, several "repeated" B-scans should be compared for reliable distinction between the stable "solid" pixels and variable faster decorrelating "liquid" pixels; this methodology is prone to natural bulk motions of living tissue [15]. For example, in typical realizations of the SV approach, the decorrelation times of blood in vessels on the order 10^1–10^2 ms require ~8 repeated B-scans in a stack [14,15], since typical B-scan frame rates range from several to several tens of Hz. Technological improvements enabling higher frame rates may decrease the bulk tissue motion artifacts, but may also decrease the SV microvascular contrast because of insufficient decorrelation during the inter-frame interval. Thus, the current compromise is to physically stabilize the interrogated tissue and/or attempt to eliminate the bulk motion artifacts via postprocessing. Another potential drawback of SV and CM inter-B-scan analysis techniques is that all strongly decorrelated speckles in the resultant microvascular images look similar and do not retain information on decorrelation time differences of different vessels.

Here, we propose a novel 3D angiographic approach which combines elements of Doppler-based and SV methods based on amplitude and phase variability of speckles corresponding to moving scatterers in blood compared to a more "stable" background bulk tissue. The approach represents reference-free processing of individual complex signal B-scans in which the horizontal step between the adjacent A-scans is significantly smaller than the optical beam diameter. In view of such features, we refer to this as an "M-mode-like speckle variability" (MMLSV) approach. The contrast mechanism here is similar to previous SV/CM methods, but signal acquisition/analysis is different; in image regions corresponding to the blood vessels, the complex field experiences higher spatio-temporal variability (comprising both its amplitude and phase), whereas for fragments of densely spaced A-scans corresponding to

"solid" tissue, the structure of complex field pixels is almost identical. The proposed MMLSV method thus combines the contrast mechanisms used in SV/CM and Doppler OCT, which makes the method favorable for its sensitivity and robustness. However, the single densely sampled complex B-scan processing in MMLSV is significantly distinct from the previous methods in which the variability of the complex field within vessels is detected by direct comparison of amplitudes/phases of either corresponding individual pixels or small groups of pixels in consecutively obtained B-scans in the same plane (SV and CM methods), or in preselected pairs/small groups of closely located A-scans in a B-scan (Doppler methods). Here, MMLSV analyzes the variability of the complex field in each single dense B-scan by evaluating (in an integral sense) groups of closely located A-scans via high-pass filtering (HPF) of horizontal spatial Fourier components. This filtering makes it possible to preferentially segment out regions of increased complex field variability corresponding to flow and/or Brownian motion of blood scatterers in the microvasculature. Further, by varying the threshold frequency of this HPF, the regions with different degrees of complex speckle variability can be detected, making it possible to grade faster/slower decorrelating vessels. Note that the HPF does not single out the Doppler optical components of the signal per se, but rather serves to detect overall temporal signal variations because the amplitude/phase variability of speckles along the horizontal coordinate in strongly oversampled B-scans can also be because of transverse flows and even Brownian motions of scatterers, similar to other speckle contrast methods.

The essence of the proposed MMLSV approach is illustrated in Fig. 1, where panel (a) schematically shows a stack of B-scans with strongly overlapped A-scans filling the inspected three-dimensional volume. The experimental B-scan on the top of panel (d) illustrates that, indeed, in such dense B-scans, the motionless scatterers in the structural image look like horizontally elongated speckles (shown as "long dashes" in the corresponding schematic below). The encircled region in this B-scan fragment shows a vessel cross section with moving scatterers (erythrocytes and other blood cells). This motion causes faster varying speckles that are much shorter in the horizontal direction along the B-scan ("short-dash" speckles in the schematic below). The horizontal spatial spectrum of the shorter dashes thus extends to higher spatial frequencies. Consequently, applying high-pass filtering to such strongly oversampled B-scans predominantly retains higher variability "short-dash" speckles representing moving scatterers. Panel (c) shows that, by changing the threshold frequency of the high-pass filter, areas with faster and slower varying pixels can be distinguished; this leads to vessel gradation/flow quantification as discussed below (Fig. 2). After performing inverse Fourier transform, the filtered B-scan exhibits only the regions corresponding to blood-containing faster varying speckles [panel (e) filtered experimental image on top and schematic on bottom]. The entire stack of processed B-scans (panel (g)) enables three-dimensional visualization of the microvasculature. Resultant three-dimensional images can be color-encoded to represent vessels with higher/lower temporal variability (analogous to band-pass Doppler OCT [7]), or to encode depth (similar to other vasculature imaging methods [14,15]). The depth-encoded result is displayed in panel (f), along with a photograph of the dorsal window chamber in a mouse showing the location of the imaged volume. Once again, note that the difference between high and low frequency components is not related to the Doppler shift of optical frequencies, but rather indicates a different rate of variability of speckles. For the motionless scatterers, this is determined by the time required for the scanning optical beam to cover its own diameter, and the motion of scatterers further reduces this characteristic time (as in SV methods).

Another important and inherently advantageous step of image processing in MMLSV is illustrated in Fig. 1(b), allowing for rather efficient compensation of natural bulk

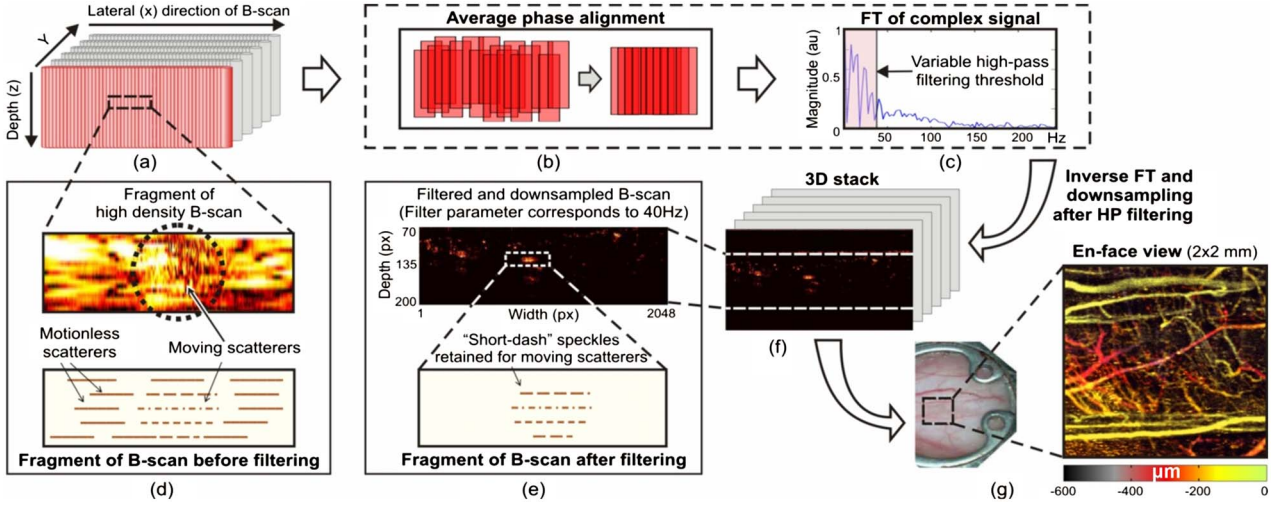

Fig. 1. Principle of operation of the MMLSV approach: (a), a stack of dense B-scans with strongly overlapped A-scans; (b) a single B-scan before and after equalization of average phases of neighboring A-scans; (c) a spatial spectrum of a single horizontal array of pixels in a dense B-scan, where low-frequency components correspond to slowly varying motionless scatterers; (d) an experimental B-scan fragment with an encircled region of rapidly varying speckles corresponding to a vessel cross section (top) and a schematic B-scan with speckles slowly and rapidly varying in the horizontal direction (bottom); (e) the same as (d), but after high-pass filtering (only vessel cross sections are now visible); (f) a photo of a mouse dorsal window chamber and an example of *en face* depth-encoded view of a 2 mm × 2 mm (lateral) 0–0.6 mm (depth) region of the detected mouse microvasculature.

tissue motions. Because of the relatively small interval between A-scans, the axial displacements ("clutter") remain smaller than the quarter of optical wavelength for bulk motion velocities up to ~several cm/s. Determining the phase difference $[\varphi_{n+1} - \varphi_n]_{\text{aver}}$ for the entire neighboring A-scans numbered n and $n+1$ (e.g., using the Kasai estimator [23]), the averaged phase differences can be compensated, so that the equalized phase $\varphi_{n+1}(i)_{\text{eq}}$ of i_{th} pixel in $(n+1)_{\text{th}}$ A-scan becomes

$$\varphi_{n+1}(i)_{\text{eq}} = \varphi_{n+1}(i) - [\varphi_{n+1} - \varphi_n]_{\text{aver}}.$$

Such equalization (see also [19,20,24,25]) ensures significantly higher stability of the complex field signal produced by the scatterers in the "solid" tissue. Importantly, for the small portions of A-scans corresponding to blood vessel cross sections, such phase equalization over the entire A-scans does *not* cancel the variations of the complex signal from scatterers moving in the liquid, so that the vessel "signal" is not degraded; the masking influence of the *axial* bulk motions can thus be effectively reduced up to axial velocities ~cm/s (estimated as half-wavelength ~0.5–1 μm divided by an inter-A-scan interval of $\sim 10^{-4}$–10^{-5} s). Concerning the tolerance to *lateral* clutter motions, the signal from "solid" pixels remains fairly stable, even if horizontal displacements are comparable with the optical beam diameter during the interval of analysis (~ the number of nearly overlapped A-scans divided by the A-scan rate). In the MMLSV method (analogous to the conventional speckle contrast approaches), a possible decrease in the interval of analysis is limited by the necessity of obtaining noticeable decorrelation of "liquid" pixels, and thus should not be smaller than 5–10 ms. For such intervals and optical beam width of ~20 μm, allowable horizontal velocities of bulk motions can reach several mm/s without special horizontal compensation, i.e., comparable with the above estimated axial velocity. In contrast, conventional CM/SV methods [7,14,15] require bulk motion compensation between entire B-scans separated by similar and even greater intervals. For such time steps, axial motions (which are easily compensated in the MMLSV method) can produce many-period phase ambiguity that worsens resultant compensation quality for entire B-scans.

The above described methodology generates images that are initially highly oversampled in the horizontal plane. For visualization, they can be down-sampled to the natural horizontal resolution of the OCT scanner, as determined by the optical beam diameter. Thus, another advantage of MMLSV approach is that the resolution of resultant microvascular images is the same as the OCT system's structural images (i.e., not compromised by the correlation window size as in CM methods).

For experimental demonstrations of the MMLSV method, we used a homebuilt Fourier domain OCT scanner with the central optical wavelength $\lambda = 1.32$ μm, a bandwidth of 106 nm, and a rate of 20 kHz for spectral fringes yielding 10 kHz rate of the formed and visualized complex valued (i.e., composed of two quadrature components) A-scans. The axial and lateral resolutions of the system are 10 and 20 μm. In the depth direction, the A-scans contained 256 pixels and the chosen number of B-scans for 3D scanning also equaled 256. For such parameters, phase equalization [Fig. 1(b)] ensures rather efficient compensation of bulk tissue motions with characteristic velocities ~0.5 cm/s (for frequencies ~5–10 Hz; this corresponds to displacement amplitudes ~0.2–0.1 mm).

For the examples illustrated below, the density of complex A-scans within a B-mode scan is 16,384 A-scan/mm. For this regime, the *en face* area of 2×2 mm^2 required ~13 min scanning time, which is quite long but can be additionally optimized. The number of overlapped A-scans divided by their rate determines the maximal intervals for observing speckle variability; for the discussed regime, this is ~30 ms. Thus, the observable characteristic times of speckle variability related to intrinsic motions in "liquid" pixels should be smaller than this interval. Evidently, denser overlapping increases sensitivity to slowly decorrelating vessels, but increases the scanning time.

Figure 2 shows some examples of *en face* depth-encoded images obtained by applying different threshold frequencies for high-pass filtering of oversampled B-scans, followed by down-sampling to the natural lateral resolution of the OCT scanner. All animal procedures were performed in accordance with the approved Animal Use Protocol at the Nizhny Novgorod State Medical Academy (NNSMA). In these experiments, we used BalbC mice with implanted dorsal window chambers (similar to [14,15]). To emphasize the method's robustness, we note that when the examples shown in Fig. 2 were recorded, the mouse's skin exhibited significant natural motions both in axial and lateral directions (see the video in supplementary Media 1), because there was a gap beneath the window glass allowing for free motion of the living tissue. Yet the applied compensation technique ensured successful angiographic imaging, even in this challenging setting. Another video shows another example of avascular image (maximum intensity projection) superposed with the corresponding photographic image (see Media 2).

Note that the finite number of overlapping A-scans means that even speckles corresponding to motionless scatterers exhibit variability along the B-scan, which for the examples in Fig. 2, corresponds to the ultimately low temporal variability rate $F_{\text{ult}} \sim 30$ Hz. By this reason, for HPF threshold $F_{\text{min}} = 30\ \text{Hz} \sim F_{\text{ult}}$, the bulk tissue begins to degrade the angiographic image. Choosing $F_{\text{min}} > F_{\text{ult}}$ predominantly retains image regions with characteristic variability intervals (decorrelation times) smaller than $1/F_{\text{min}}$. Figure 2 shows that, by decreasing F_{min} toward F_{ult}, slower decorrelating vessels can be visualized (although the noise from motionless/slower moving background gradually increases). The rate of this decorrelation is determined by both regular (convective) flows in a vessel and the Brownian scatterer (erythrocyte) motion (that dominates in SV imaging [14]). This fact impedes the straightforward usage of simplified arguments [26] based on the assumption of scatterer motion as in a moving solid body to link the flow and speckle variability.

In this context, one can point out two potentially relevant characteristic times: (1) $\sim D/V_{\text{sc}}$, for a scatterer moving with velocity V_{sc} crossing the beam diameter D, and (2) $\sim \lambda/4V_{\text{sc}}^{\text{rel}}$ during which the axial distance between a pair of subresolution scatterers having the relative axial velocity $V_{\text{sc}}^{\text{rel}}$ varies by a quarter of wavelength $\lambda/4$. Such a variation also can cause speckle blinking in the image [22]. For parameters used in obtaining Fig. 2, characteristic values for V_{sc} and $V_{\text{sc}}^{\text{rel}}$ differ by ~20 times and,

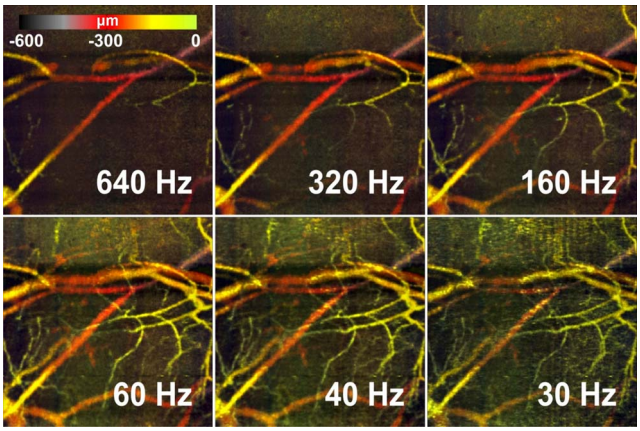

Fig. 2. Examples of color depth encoded *en face* microvascular images obtained for different filter thresholds F_{min}, demonstrating the gradual appearance of finer vessels with different rates of speckle variability. Presumably, for the highest $F_{min} > 160$ Hz, the contributions of faster flows are dominant (first arterioles and then venules), whereas for $F_{min} \sim 40$–60 Hz, the slower regions of flow and possibly the Brownian scatterer motion in finer microvessels (~ capillaries) contribute to the angiographic image. The signal from the motionless background tissue begins to degrade the image quality at $F_{min} = 30$ Hz. FOV = 2 mm × 2 mm for all panels. A video record showing significant bulk motions of the tissue while obtaining these images is given in Media 1. Another example of a vascular image (maximum intensity projection) superposed with the corresponding photographic image is given in Media 2.

depending on F_{min}, fall into the range from fractions mm/s to several mm/s, which is realistic for Brownian motion and collective (convective) flow velocities.

Overall, the MMLSV approach is hybrid and exhibits certain features of Doppler and phase-resolved methods that compare pixel phases in individual A-scans (or use other ways to estimate Doppler frequency components, for example spectral filtering). From the viewpoint of scanning, MMLSV is close to the M-mode, whereas the use of speckle variability resembles elements of SV/CM methods, although here the comparison is made within each dense B-scan rather than between repeated B-scans from the same position. The use of both amplitude and phase information in MMLSV-OCT further enhances the positive features of both classes of microvascular OCT methods mentioned above. Note that the utility of combining analogous techniques is also shown in recent work [27] using a two-stage combined processing. Rapid aligning of relatively small groups of strongly overlapped A-scans significantly improves the tolerance of MMLSV-OCT to bulk tissue motion. Although the tradeoff for this is a noticeable increase in total scanning time compared with inter-B-scan SV/CM methods [14,15]), in many cases, robustness to bulk motion artifacts may be more important, and thus a longer total imaging time may be acceptable. Besides, quantification of blood vessels in terms of faster/slower decorrelations is also naturally enabled through the user selected cutoff frequency of the high-pass filtering, and may be linked to physiologically important dynamic variables such as flow velocity and perfusion. This, and the separation of flow versus Brownian motion contributions to the MMLSV signal, represent interesting challenges that will be addressed in future publications.

This work was supported by the grant of the Russian Federation Government no. 14.B25.31.0015 and RFBR grant no. 15-42-02513. VYZ and VMG acknowledge partial support by the grant no. 02.B49.21.0003 of the Russian Ministry of Education.

References

1. B. F. Kennedy, K. M. Kennedy, and D. D. Sampson, IEEE J. Sel. Top. Quantum Electron. **20**, 272 (2014).
2. T. Marvdashti, L. Duan, K. L. Lurie, G. T. Smith, and A. K. Ellerbee, Opt. Lett. **39**, 5507 (2014).
3. V. Y. Zaitsev, V. M. Gelikonov, L. A. Matveev, G. V. Gelikonov, A. L. Matveyev, P. A. Shilyagin, and I. A. Vitkin, Radiophys. Quantum Electron. **57**, 52 (2014).
4. S. Wang, K. V. Larin, J. Li, S. Vantipalli, R. K. Manapuram, S. Aglyamov, S. Emelianov, and M. D. Twa, Laser Phys. Lett. **10**, 075605 (2013).
5. J. Li, S. Wang, M. Singh, S. Aglyamov, S. Emelianov, M. D. Twa, and K. V. Larin, Laser Phys. Lett. **11**, 065601 (2014).
6. R. Leitgeb, L. Schmetterer, W. Drexler, A. Fercher, R. Zawadzki, and T. Bajraszewski, Opt. Express **11**, 3116 (2003).
7. V. X. D. Yang, M. L. Gordon, B. Qi, J. Pekar, S. Lo, E. Seng-Yue, A. Mok, B. C. Wilson, and I. A. Vitkin, Opt. Express **11**, 794 (2003).
8. R. K. Wang, S. L. Jacques, Z. Ma, S. Hurst, S. R. Hanson, and A. Gruber, Opt. Express **15**, 4083 (2007).
9. M. Szkulmowski, A. Szkulmowska, T. Bajraszewski, A. Kowalczyk, and M. Wojtkowski, Opt. Express **16**, 6008 (2008).
10. R. K. Wang and L. An, Opt. Express **17**, 8926 (2009).
11. R. K. Wang, IEEE J. Sel. Top. Quantum Electron. **16**, 545 (2010).
12. E. Jonathan, J. Enfield, and M. J. Leahy, J. Biophotonics **4**, 293 (2011).
13. K. Kurokawa, K. Sasaki, S. Makita, Y. J. Hong, and Y. Yasuno, Opt. Express **20**, 22796 (2012).
14. A. Mariampillai, B. A. Standish, E. H. Moriyama, M. Khurana, N. R. Munce, M. K. K. Leung, J. Jiang, A. Cable, B. C. Wilson, I. A. Vitkin, and V. X. D. Yang, Opt. Lett. **33**, 1530 (2008).
15. A. Mariampillai, M. K. K. Leung, M. Jarvi, B. A. Standish, K. Lee, B. C. Wilson, A. Vitkin, and V. X. D. Yang, Opt. Lett. **35**, 1257 (2010).
16. Y. K. Tao, A. M. Davis, and J. A. Izatt, Opt. Express **16**, 12350 (2008).
17. S. Yousefi, J. Qin, and R. K. Wang, Biomed. Opt. Express **4**, 1214 (2013).
18. Y. Jia, O. Tan, J. Tokayer, B. Potsaid, Y. Wang, J. J. Liu, M. F. Kraus, H. Subhash, J. G. Fujimoto, J. Hornegger, and D. Huang, Opt. Express **20**, 4710 (2012).
19. V. Srinivasan, J. Jiang, M. Yaseen, H. Radhakrishnan, W. Wu, S. Barry, A. E. Cable, and D. A. Boas, Opt. Lett. **35**, 43 (2010).
20. J. Lee, V. Srinivasan, H. Radhakrishnan, and D. A. Boas, Opt. Express **19**, 21258 (2011).
21. M. S. Mahmud, D. W. Cadotte, B. Vuong, C. Sun, T. W. H. Luk, A. Mariampillai, and V. X. D. Yang, J. Biomed. Opt. **18**, 050901 (2013).
22. V. Y. Zaitsev, I. A. Vitkin, L. A. Matveev, V. M. Gelikonov, A. L. Matveyev, and G. V. Gelikonov, Radiophys. Quantum Electron. **57**, 210 (2014).
23. C. Kasai, K. Namekawa, A. Koyano, and R. Omoto, IEEE Trans. Son. Ultrason. **32**, 458 (1985).
24. J. Fingler, D. Schwartz, C. Yang, and S. E. Fraser, Opt. Express **15**, 12636 (2007).
25. A. A. Moiseev, G. V. Gelikonov, D. A. Terpelov, P. A. Shilyagin, and V. M. Gelikonov, Laser Phys. Lett. **9**, 826 (2012).
26. N. Mohan and B. Vakoc, Opt. Lett. **36**, 2068 (2011).
27. W. J. Choi, R. Reif, S. Yousefi, and R. K. Wang, J. Biomed. Opt. **19**, 036010 (2014).